Design of the heat exchanger for Passive Molten Salt Fast Reactor using GAMMA+ code

Dowon Lee[a], Juhyeong Lee[a], Seungmin Lee[a], Jihun Im[a], JinHo Song[a], Sung Joong Kim[*a,b]
[a]*Department of Nuclear Engineering, Hanyang University*
222 Wangsimni-ro, Seongdong-gu, Seoul 04763, Republic of Korea
[b]*Institute of Nano Science and Technology, Hanyang University*
222 Wangsimni-ro, Seongdong-gu, Seoul 04763, Republic of Korea
[*]*Corresponding author: sungjkim@hanyang.ac.kr*

Keywords : Molten salt reactor, GAMMA+, Helical shell and tube heat exchanger, Optimization of heat exchanger

1. Introduction

Molten salt reactors (MSRs) are in the spotlight because of their safety features, high energy efficiencies, and carbon neutrality. According to these benefits, many countries are interested in MSRs development [1]. The I-SAFE-MSR Research Center in South Korea is designing a Passive Molten Salt Fast Reactor (PMFR). The PMFR adopts natural circulation in primary loop to exclude mechanical pumps because of its enhancement of safety characteristics.

Heat exchanger (HX) is crucial for deciding the possibility of natural circulation concept in PMFR. Also, the HX volume determines the total mass of fuel salt, which is related to the operation cost of the reactor. Therefore, an appropriate and optimized design of the HX is essential.

The HX design of PMFR is considered the helical shell and tube type, inspired by NuScale and SMART [2-3]. Helical shell and tube type HXs have the advantages of substantial heat transfer efficiency, suitability of high temperature, and compactness for minimizing the volume of a HX.

This study aims to design a helical shell and tube HX by analyzing the number of transversal tubes, considering both system-integrated and modular configurations. The height is fixed at 5m to maintain a compact system layout. Additionally, maintaining a sufficient height difference between the core and the HX keeps the thermal center elevated, thereby enhancing the natural circulation driving force.

To evaluate the thermal performance and design feasibility of the proposed HX configurations, a sensitivity analysis on the number of transversal tubes was conducted using the GAMMA+ code. Originally developed at KAERI for the design and safety analysis of high temperature gas cooled reactors, GAMMA+ has been extended to support next-generation reactors, including MSRs [4].

2. Modeling of PMFR

In this section, the nodalization of the PMFR and the thermal-hydraulic correlations used in GAMMA+ are introduced.

2.1 PMFR and helical HX Model

Fig. 1 shows the configurations of the PMFR designed with a system-integrated HX and a modular HX, respectively. The primary loop of the reactor consists of the lower plenum, core, riser, upper plenum, primary HX and downcomer, with an off-gas system applied at the top. In this study, a total of six modular HXs were assumed. The number of modules is related to the fuel salt volume and heat exchange capacity, requiring a sensitivity analysis, which will be conducted as part of future work.

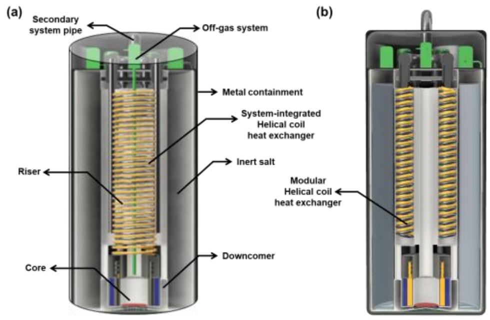

Fig. 1. Schematic of PMFR (a) system-integrated HX and (b) Modular HX

Fig. 2 illustrates the nodalization for (a) and (b) of **Fig. 1**, respectively. The heat generated in the core is incorporated as a power distribution for each node, reflecting the previous PMFR core analysis results [5]. $NaCl\text{-}KCl\text{-}UCl_3$ is chosen as the fuel salt due to its low melting point and suitability for long term operation. $NaCl\text{-}MgCl_2$ is used as the secondary coolant salt, and the thermophysical properties of both salts are taken from the built-in data in GAMMA+. For the secondary side, in case of the system-integrated HX, the inlet temperature is set to 460 °C, and the mass flow rate is set to 1500 kg/s. In contrast, for the modular HX, an inlet temperature of 460 °C and a mass flow rate of 250 kg/s are applied. For the simplification of the analysis, heat transfer is assumed to occur only within the HX region, and heat losses are excluded from the analysis.

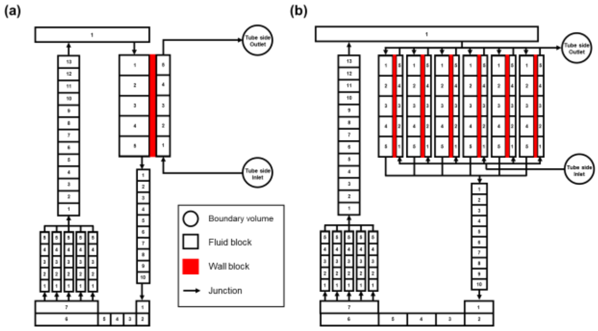

Fig. 2. Nodalization of PMFR in GAMMA+ (a) system-integrated HX and (b) Modular HX

The structure of helical shell and tube HX and parameters are shown in **Fig. 3**. To maximize the heat exchange efficiency, the fuel salt flows downward in the shell, while the coolant salt rises in the tube, selecting a counterflow design. The system-integrated HX is composed of a concentric cylindrical structure, and the modular HX is made up of a cylinder configuration. There are two types of tube arrangements, in-line and staggered. In the PMFR, the staggered arrangement is used. The criterion for comparing the two configurations was volume minimization, where the volume was calculated as the difference between the shell volume and the tube volume, as shown in the figure below.

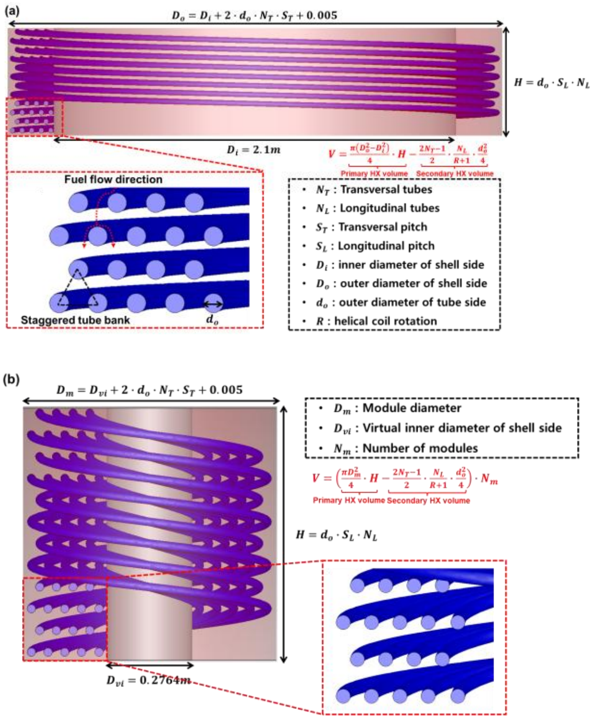

Fig. 3. Helical shell and tube HX schematic and parameters (a) system-integrated HX (b) modular HX

2.2 Hydraulic model

GAMMA+ includes pressure drop and heat transfer modeling for each geometry, and in this study, cylinder, concentric pipe, and helical shell and tube geometries were used. The embedded thermal hydraulic model was compared with the literature, and the differences were corrected using a multiplier. Additionally, the form loss coefficient is taken as an input parameter based on literature references.

2.2.1 Pressure drop correlation

For the pressure drop model, the Zukauskas correlation was used for the shell side, and the Mori-Nakayama correlation was used for the tube side [6-7]. While there was no difference between the GAMMA+ result and the literature for the tube side, a discrepancy was observed for the shell side. Eq. (1) represents the pressure drop on the shell side as presented in GAMMA+, while Eqs. (2) and (3) express the pressure drop models for the shell side that are consistent with the PMFR HX specifications from the literature. In Eq. 1, N denotes the number of transversal tubes, χ is the correction factor, K_D is defined as $f \cdot \frac{L}{D_h}$, A_r denotes $\frac{A_{avg}}{A_{min}}$ derived from the mass flow rate equation, and η is a multiplier which is expressed as $N \cdot \chi$. In Eqs. (2) and (3), Eu is a function of the transversal pitch to diameter ratio (P/D) and the Reynolds number for the staggered tube arrangement. The coefficient k_1 is set to 1 for the equilateral triangular layout, which is applied in the PMFR HX configuration. The multiplier in Eq. (4) was derived from Eqs. (1) and (2).

$$\Delta P = N \cdot \chi \cdot \left(\frac{1}{2}\rho V_{max}^2\right) \cdot K_D = \eta \cdot (A_r^2) \cdot \left(\frac{1}{2}\rho V_{avg}^2\right) \cdot K_D \tag{1}$$

$$\Delta P = Eu \cdot \left(\frac{1}{2}\rho V_{max}^2\right) \cdot N = Eu \cdot (A_r^2) \cdot \left(\frac{1}{2}\rho V_{avg}^2\right) \cdot N \tag{2}$$

$$\frac{Eu}{k_1} = 0.162 + \frac{0.181 \cdot 10^4}{Re} + \frac{0.792 \cdot 10^8}{Re^2} - \frac{0.165 \cdot 10^{13}}{Re^3} + \frac{0.872 \cdot 10^{16}}{Re^4} \tag{3}$$

$$\eta = N \cdot \frac{Eu}{K_D} \tag{4}$$

Eq. (5) shows the pressure drop correlation on the tube side, where d_i represents the inner diameter of the tube and D_c is the diameter of the coil wound around the concentric cylinder, which is calculated as $\frac{D_i+D_o}{2}$.

$$f = \left(\frac{d_i}{D_c}\right)^2 \cdot \frac{0.192}{\left[Re\left(\frac{d_i}{D_c}\right)^{2.5}\right]^{\frac{1}{6}}} \left\{1 + \frac{0.068}{\left[Re\left(\frac{d_i}{D_c}\right)^{2.5}\right]^{\frac{1}{6}}}\right\} \tag{5}$$

2.2.2 Heat transfer correlation

Like the pressure drop model, the heat transfer model employs the Zukauskas correlation for the shell side and the Mori-Nakayama correlation for the tube side. While the shell side model in GAMMA+ differs from the literature, the tube side model is identical to that reported in previous studies. Eq. (6) is the correlation presented in GAMMA+, and the unknown coefficients are determined by the tube arrangement and the maximum Reynolds number on the shell side. In this study, C is set to 0.40, m to 0.60, and n to 0.36, which were selected based on the results from applying a staggered tube arrangement. Eq. (7) is the correlation from the literature suitable for the PMFR, and the multiplier was derived using the two equations, which is summarized in Eq. (8). In Eqs. (6) to (8), Pr_b denotes the Prandtl number of the fuel salt, and Pr_w represents the Prandtl number at the wall. Re_{max} and Re_{avg} is the maximum and average Reynolds number on the shell side respectively, while a and b refer to transversal and longitudinal P/D, respectively. Moreover, the heat transfer modeling for the tube side is presented in Eq. (9).

$$Nu = C(Re_{max})^m (Pr_b)^n \left(\frac{Pr_b}{Pr_w}\right), \; Re_{max} = A_r \left(\frac{\rho v_{avg} D_h}{\mu}\right) = A_r \cdot Re_{avg} \quad (6)$$

$$Nu = 0.35 \cdot \left(\frac{a}{b}\right)^{0.2} (Re_{avg})^{0.60} (Pr_b)^{0.36} \left(\frac{Pr_b}{Pr_w}\right)^{0.25} \quad (7)$$

$$\eta = \frac{0.35}{0.40} \cdot \left(\frac{a}{b}\right)^{0.2} \cdot A_r^{-m} \cdot \left(\frac{Pr_b}{Pr_w}\right)^{-0.75} \quad (8)$$

$$Nu \cdot Pr_b^{-0.4} = \frac{1}{41.0} Re^{\frac{5}{6}} \left(\frac{d_i}{D_c}\right)^{\frac{1}{12}} \cdot \left[1 + \frac{0.061}{\left\{Re\left(\frac{d_i}{D_c}\right)^{2.5}\right\}^{\frac{1}{6}}}\right] \quad (9)$$

2.2.3 Form loss coefficient

For the form loss term, a standard 90° elbow ($K_{loss} = 0.7$) was applied between node 1 and 2 of the lower plenum, accounting for geometric changes within the same fluid block. In addition, form loss coefficient caused by area changes at the junctions between different fluid blocks specifically, sudden expansion and sudden contraction were also considered. The corresponding loss terms were referenced from the literature, and for the contraction case, a curve fitting was performed based on a figure provided in reference [8]. Equation (10) and (11) represent the form loss correlation for sudden expansion and contraction, respectively.

$$K_{SE} = \left(1 - \frac{A_1}{A_2}\right)^2 = \left(1 - \frac{d^2}{D^2}\right)^2 \quad (10)$$

$$K_{SC} = 1.41e^{-0.48\left(\frac{A_2}{A_1}\right)} - 0.89 \quad (11)$$

2.3 Node sensitivity study

A node sensitivity analysis was conducted to determine the appropriate number of nodes for the HX. In the steady state analysis, the inlet and outlet temperature on the shell side of the HX were selected as the reference variables. The results for each nodal configuration are presented in **Table 1**. The inlet and outlet temperature of the primary HX exhibited minimal variation with respect to the number of nodes. Therefore, the number of nodes was determined to be 5.

Table 1: Node sensitivity analysis

	$T_{h.in}$ / $T_{h.out}$ (°C)	Relative error (%)
5 nodes	647.640 / 534.634	0.087 / 0.026
10 nodes	647.075 / 534.775	0.030 / 0.008
15 nodes	646.881 / 534.816	0.013 / 0.004
20 nodes	646.794 / 534.839	-

2.4 Methodology and test matrix

The system parameters used in the design of system-integrated and modular HXs are summarized in **Table 2**.

Table 2: Design parameters of PMFR in GAMMA+

Parameters	**Values**
Reactor	
Core diameter	2 m
Core height	1.95 m
Riser diameter	0.6 m
Riser height	13.05 m
Thermal output	200 MWth
Heat exchanger	
Heat exchanger height	5 m
Tubes outer diameter	9.525 mm / 15 mm / 25 mm
Tubes inner diameter	7.525 mm / 13 mm / 23 mm
Transversal P/D	2.0
Longitudinal P/D	$\sqrt{3}$
Transversal tube rows	**Sensitivity**
Longitudinal tube rows	Number corresponding to 5 m
Tube material	Hastelloy-N
Tube thermal conductivity	20 W/m·K
Tube volumetric heat capacity	-214.844·T+5.144·10⁶ J/m³·K

The outer diameter of the tubes was selected based on the MSBR, and since the tube diameter is related to both heat exchange efficiency and the pressure drop on the secondary side, it was varied and analyzed. For the two types of HXs, cases were investigated by varying both the number of transversal tubes and the number of helical coil rotations. The analysis was performed under the following conditions: the pressure drop on the secondary side remained below 2 MPa, the inlet temperature of the fuel salt HX was below 650 °C and the outlet temperature exceeded 500 °C. The inlet temperature of shell side HX was set to ensure reactor criticality, while the outlet temperature was determined to maintain a sufficient margin from the fuel salt's solidification point. The pressure drop limit on the secondary side was set during the preliminary analysis based on the specifications of the available mechanical pumps, and its detailed determination through comprehensive literature review and evaluation is left for future work. Using the following algorithm, the HX design with the smallest volume from each case was selected as the optimal configuration. The methodology is illustrated in **Fig. 4**.

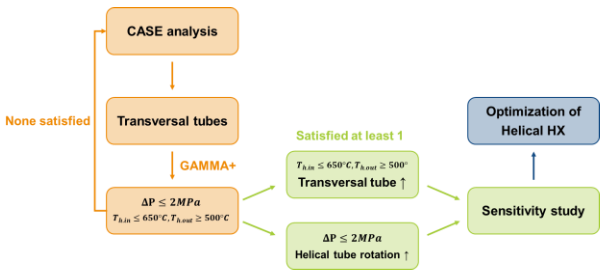

Fig. 4. Design methodology for the helical shell and tube HX

Table 3 presents the test matrix, which was constructed for a total of 6 cases based on three different tube outer diameters and two types of HXs, as described in **Table 2**.

Table 3: Test Matrix

d_o / d_i \ ***H***	**System-integrated HX**	**Modular HX**
$25mm$ / $23mm$	CASE 01	CASE 02
$15mm$ / $13mm$	CASE 03	CASE 04
$9.525mm$ / $7.525mm$	CASE 05	CASE 06

3. Results and Discussion

Fig. 5 presents the HX designs of CASE 01 and CASE 02. R represents the number of helical coil rotations illustrated in **Fig. 3**. The red dashed line represents the 2 MPa reference line, and the blue dashed line indicates the 650 °C reference line. Cases located below both dashed lines are considered feasible HX designs. Among these, the case with the smallest number of transversal tubes exhibits the smallest outer diameter of shell side HX and is therefore identified as the optimal design. For CASE 01, the optimal design was derived from 33 transversal tubes and an R value of 9, resulting in a volume of 80.9699 m^3. The optimal design for CASE 02, comprising 14 transversal tubes and an R value of 22, yielded a calculated volume of 52.8620 m^3.

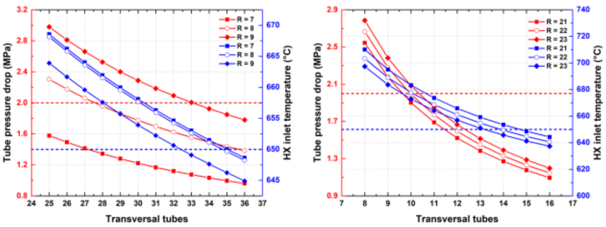

Fig. 5. CASE 01 and CASE 02 HX design results

The results of CASE 03 and CASE 04, derived using the same methodology as in the preceding analyses, are presented in **Fig. 6**. In CASE 03, all configurations with an R value of 5 exhibited tube side pressure drops exceeding 2 MPa threshold. While increasing the number of transversal tubes at an R value 5 allowed the pressure drop constraint to be satisfied, the resulting increase in HX volume rendered these configurations suboptimal. Therefore, no feasible design meeting both hydraulic and volumetric criteria was identified for this case. In contrast, the optimal design was found when the R value was 4 and the number of transversal tubes was 27, with a volume of 30.1746 m^3. For CASE 04, the optimal design was obtained when the R value was 13 and the number of transversal tubes was 11, resulting in a volume of 17.3536 m^3.

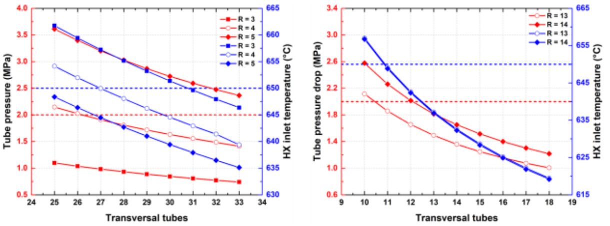

Fig. 6. CASE 03 and CASE 04 HX design results

Fig. 7 presents the results for CASE 05 and CASE 06. For CASE 05, no cases achieved convergence when the R value was 1. This is due to the large ascent angle, which reduces the helical coil path length and fails to provide sufficient heat transfer area. Additionally, when the R value was 3, there were no cases with a tube pressure drop below 2 MPa. Therefore, the optimal design was determined when the R value was 2 and the number of transversal tubes was 28, with an optimal volume of 18.6385 m^3. For CASE 06, the optimal HX design was derived when the number of transversal tubes was 14 and the R value was 8, with a volume of 12.5896 m^3. In all cases, the outlet temperature of the fuel salt HX remained above 500 °C, indicating a sufficient margin from the salt solidification point.

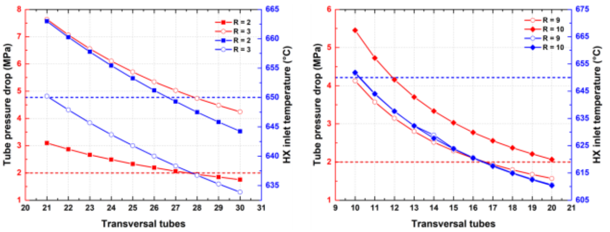

Fig. 7. CASE 05 and CASE 06 HX design results

Table 3 summarizes the optimal HX volumes for each case, with CASE 06 having the smallest volume. The optimal HX volume decreases as the tube's outer diameter becomes smaller. This occurs because tube outer diameter determines the concentric pipe outer diameter in system-integrated HX, and cylinder diameter of modular HX. Furthermore, for the same tube diameter, the optimal design volume of modular HX was smaller than that of system-integrated HX. This is because the modular HX has higher heat exchange efficiency than the system-integrated HX when comparing heat transfer area and primary HX inlet temperature, allowing for sufficient heat removal even with a smaller volume. The HX inlet temperature and heat transfer area for each optimal design cases are presented in **Fig. 8**. Additionally, as the tube diameter decreases, the heat transfer efficiency increases, causing a larger difference in HX inlet temperature compared to the heat transfer area, as observed in CASE 04 and CASE 06.

Table 3: Optimal helical HX volume for each case

d_o / d_i \ ***H***	**System-integrated HX**	**Modular HX**
$25\ mm$ / $23\ mm$	80.9699 m^3	52.8620 m^3

$15\ mm\ /\ 13\ mm$	30.1746 m^3	17.3536 m^3
$9.525\ mm\ /\ 7.525\ mm$	18.6385 m^3	12.5896 m^3

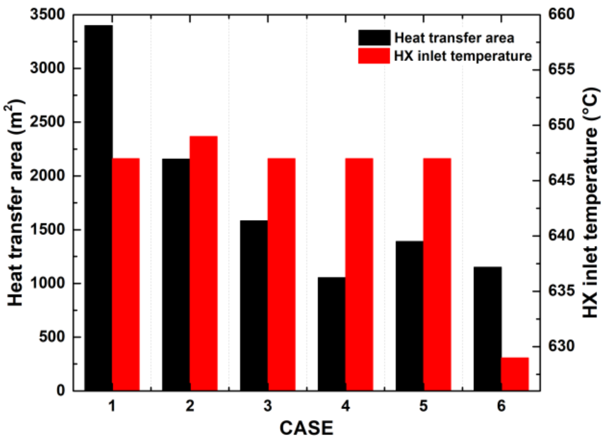

Fig. 8. Heat transfer area and HX inlet temperature in the optimal HX design from CASE 01 to CASE 06

4. Conclusion

In this study, system-integrated HX and modular HX were designed by varying the number of transversal tubes, helical coil rotations, and the outer diameter of the tubes. Among these designs, the most cost-effective HX design was derived. A total of 6 cases were conducted, and the insights gained are as follows.

- ✓ Modular HX was more advantageous than system-integrated HX in terms of volume and heat transfer efficiency
- ✓ Smaller tube diameters were more beneficial in terms of volume, as well as heat transfer efficiency
- ✓ The optimal HX volume for PMFR was 12.5896 m^3, which corresponds to the case with a tube outer diameter of 9.525 mm, 8 helical coil rotations, and 14 transversal tubes

This study designed and optimized the HX variables through a sensitivity study. Parameters such as the pressure constraint of secondary HX and the number of modules, which were defined during the preliminary analysis of the optimization process, are left for future work. Based on this methodology, the GAMMA+ code is expected to be widely applied to the HX design of MSRs.

ACKNOWLEDGEMENTS

This research was supported by the National Research Foundation of Korea (NRF) and funded by the ministry of Science, ICT, and Future Planning, Republic of Korea (grant numbers RS-2021-NR056168). Additionally, this work was also supported by the Human Resources Development of the Korea Institute of Energy Technology Evaluation and Planning (KETEP) grant funded by the Korea government Ministry of Knowledge Economy (RS-2024-00439210).

REFERENCES

[1] INTERNATIONAL ATOMIC ENERGY AGENCY, Status of Molten Salt Reactor Technology, Technical Reports Series No. 489, IAEA, Vienna (2023)

[2] U. S. Nuclear Regulatory Commission, “NuScale Power, LLC, Design Certification Application – Safety Evaluation With No Open Items for Chapter 3, ‘Design of Structures, Systems and Components and Equipment’,” January 8, 2020

[3] Park, H.-S., Kwon, T.-S., Moon, S.-K., Cho, S., Euh, D.-J., & Yi, S.-J. (2017). Contribution of thermal–hydraulic validation tests to the standard design approval of SMART. *Nuclear Engineering and Technology*, *49*(7), 1445–1455.

[4] Lim, H.S. (2014) “GAMMA+1.0 Volume II: Theory Manual,” KAERI/TR-5728/2014, KAERI

[5] Nariratri Nur Aufanni, Lee, E., Oh, T., & Kim, Y. (2023). Burnable Absorber Design Study for a Passively-Cooled Molten Salt Fast Reactor. *Nuclear Engineering and Technology*

[6] Zukauskas, A., and Romanas Ulinskas. "Heat transfer in tube banks in crossflow." (1988)

[7] Y. Mori and W. Nakayama, Study on Forced Convective Heat Transfer in Curved Pipes, Int. J. Heat Mass Transfer, Vol. 10, pp. 37-59, 1967

[8] F. M. White, Fluid Mechanics, McGraw and Hill, New York, 7th edn, 2011.